Geophys. J. R. astr. Soc. (1975) **42,** 827–857

Stress and Flow beneath Island Arcs

Norman H. Sleep

(Received 1975 February 10)*

Summary

The flow pattern, stress distribution, topography, and gravity anomalies were computed from numerical models having density and viscosity distributions resemblant to the Aleutian arc. The results were compatible with the hypothesis that the excess density of the slab drives its descent and that hydrodynamic forces are responsible for topographic and gravity highs over the outer rise seaward of the trench and the frontal arc and lows over the trench. In models with simple distributions of rheological parameters, the force from the slab was transmitted directly upward producing a negative gravity anomaly over the arc. Material with low resistance to flow was needed along the fault plane above the slab or within the crust of the frontal arc and within the wedge of asthenosphere above the slab to reduce that force and to allow the horizontal lithosphere to move with the slab. Models with the resistance to flow thus reduced had outer rises, deep trenches, horizontal tension seaward of the trench, horizontal compression under the trench, and downdip tension in the slab. Free air gravity anomalies, which are the sum of between deflections of the free surface due to hydrodynamic forces and direct attractions from the masses driving the flow, were not fit excellently by any of the models, in part because the coarse grid used precluded accurate representation of the fault zone above the slab and the frontal arc. An alternate to the hypothesis that about 5 kb of stress on the fault plane is needed to produce an outer rise is offered by these models. Shear stress between the slab and the island arc was always below 700 bars in the more successful models if the density distribution was scaled to match the topography of the trench. This is much less than the 2000 bars stresses needed if frictional heating causes island arc volcanism.

Introduction

The theory of plate tectonics, which dictates that the oceanic lithosphere, approximately 100 km thick, forms at mid-ocean ridges, moves horizontally, and returns to the Earth's interior beneath ocean trenches, has synthesized a wide range of observations from geology and geophysics. Although the relative motions are reasonably well determined, the dynamic mechanisms governing plate motion are not. In this paper, we examine possible physical processes of subduction zones to determine the importance thereof and to relate the results to the origin of the topography, stress, and gravity anomalies characteristic of these regions. Because of the complex nature of

* Received in original form 1974 October 25.

the problem numerical methods were used to quantify the results and to explicitly consider both lithospheric and asthenospheric regions. Previous numerical studies of flow in the mantle did not have sufficient resolution to be directly relevant to the observations of interest (e.g. Turcotte & Oxburgh 1969; Richter 1973) or modelled only the region outside of the slab (McKenzie 1969; Sleep & Toksöz 1971; Andrews & Sleep 1974).

The excess density probably associated with descending lithospheric plates is a likely driving force for subduction (Morgan 1965a, b; Elsasser 1967; McKenzie 1969, 1972; Turcotte & Oxburgh 1969; Jacoby 1970; Isacks & Molnar 1971; Griggs 1972; see Fig. 1). The tendency of low density continental crust of the island arc to rise and spread probably precludes its subduction or may otherwise influence the pattern of flow (McKenzie 1969; Artyushkov 1973, 1974). Force between the slab and the adjacent oceanic plate may drive the plate (and thus retard subduction) or may drive the descending slab (and thus retard the plate). One of the effects, although which is not *a priori* evident, should exist at a given location, since the entire oceanic plate moves as a unit with some parts supplying drag and others driving forces (Elsasser 1967; Solomon & Sleep 1974). The slab must also induce flow in the asthenosphere and interact with any larger scale flow patterns. The effect of driving forces and density heterogeneities may be modified by differences in the resistance to deformation between different regions within the subduction zone and by non-linear resistance to deformation where the lithosphere is strongly deformed.

A short slab, in particular the Aleutian slab near Adak and Amchitka, was considered most intensively, since the purpose was mainly to study the interactions of the lithospheric plates, the slab, and the crust of the island arc. For a longer slab, sphericity and such hypothesized effects as resistance from higher viscosity material at depth, phase changes, iron concentration gradients, and the general mantle circulation pattern produce additional complications. Computation was also minimized since more numerical grid points would be needed to represent a long slab.

The computational strategy was to calculate instantaneous flow patterns compatible with assumed density and viscosity distributions. which can be done since inertial forces are negligible in the mantle. This approach is superior at our current state of ignorance to attempting to calculate fully time dependent models. The present position of the slab can be inferred more accurately, than how subduction started and the trajectory which the slab followed. The most accurate data; elevation, topography, and earthquake mechanisms can be calculated without using time dependent models. Although no excellent fit to observed data was obtained by any of the computed models, the relative importance of various possible effects and the feasibility of hypothesis for producing topographic features and volcanism could be appraised. Certain classes of apparently reasonable models which give ludicrous results can be rejected and a calibration of the density and rheology of the slab accrues from the more successful models.

Before presenting the results of the calculations, the nature of the observations and their relevance to the problem are reviewed.

Physical parameters

In an instantaneous convection problem the input includes the distribution of density and viscosity and the nature of the boundaries to the region. Observable quantities determined from the calculation include the velocity field, non-hydrostatic stress, excess hydrostatic pressure, and viscous dissipation. The problem of determining the physical parameters and the relevant data for the Earth near subduction zones is neither simple nor straightforward. The present state of knowledge is reviewed in this section.

Kinematics of subduction

To the reader used to seeing the schematic diagrams which infest plate tectonic papers, it may appear that the slab is known to descend parallel to itself at the surface subduction rate. In fact, this has been generally assumed for simplicity in fluid dynamic models of island arcs (McKenzie 1969, 1972; Sleep & Toksöz 1971; Andrews & Sleep 1974). Upon closer inspection, it becomes evident that the kinematics beneath island arcs may be more complex and that the present streamlines (lines everywhere parallel to the flow defined mathematically in equation (A1)) need not correspond with the dip of the slab or the trajectories with which the material reached its current position. For example, if the dip of the slab increased as it grew, streamlines would cross the slab from top down.

Motion of the slab perpendicular to itself is opposed by viscous forces in the displaced asthenosphere and the resistance of the slab to deformation. A component of this motion is not precluded, however, as no rigid substrate underlies the slab and as it is unlikely that the slab is undeformable at depth while the same material was obviously deformed when it began descending. Time dependence of the flow is in fact likely, as mass and viscosity were differently distributed when the slab was shorter.

Ways of inferring the position of the slab at previous times independent of some physical assumptions are not evident. Inference of the kinematics of the asthenosphere is even more difficult. Even if the absolute velocity of the slab with respect to the underlying mantle could be calculated (see Solomon & Sleep 1974), the depth and geometry of the return flow is largely unknown. Details of flow at great depths are likely to be less important for short slabs.

Despite the problems in deducing the kinematics of the slab, certain computed models, in addition to those that give highly convoluted flow, can be rejected on kinematic grounds. It is inconsistant for the slab to descend much more rapidly than the surface subduction rate, as the slab would detach after a short period of time. In this case the slab could not have existed as assumed in the first place. Several computed models failed in this manner.

Density distribution

Convective flow depends on lateral variations in density. At first glance, it would appear the gravity anomalies might directly give this. The problem however is more complicated as hydrodynamic forces acting on the free surface may cause deflections, including oceanic trenches (Morgan 1965a, b; McKenzie 1969). On the oceanic side of the arc the unstressed position of the sea floor can be inferred from nearby sea floor. The topography which the arc would have, if the slab did not exist, is not directly evident, however. Published gravity interpretations either ignore the slab or assume its density (Grow 1973). The density structures of the crust of the island arcs obtained in these studies are therefore suspect (Watts & Talwani 1975).

The position of the down-going part of the Aleutian slab is well constrained by abundant seismic travel-time residuals from the LONGSHOT explosion (Jacob 1972; Sleep 1973). Associated amplitude anomalies (Sleep 1973), and self-consistent relocation of earthquakes observed with a local array (Engdahl 1973), have constrained the horizontal position of the slab to within at worst ± 15 km (Fig. 2). These studies also indicate that the slab does not extend significantly below the depth of the deepest earthquakes (about 220 km). The position of the relatively horizontal part of the slab between the trench and the arc is not directly constrained by this data since it is not penetrated by ray paths (Sleep 1973; Engdahl 1973) and must be inferred from the earthquake locations and mechanisms.

The approximate location of colder more dense regions can be calculated from temperature distributions which assume the kinematics of the slab (Toksöz, Sleep & Smith 1973; compare Oxburgh & Turcotte 1970, 1971). The time dependence of tem-

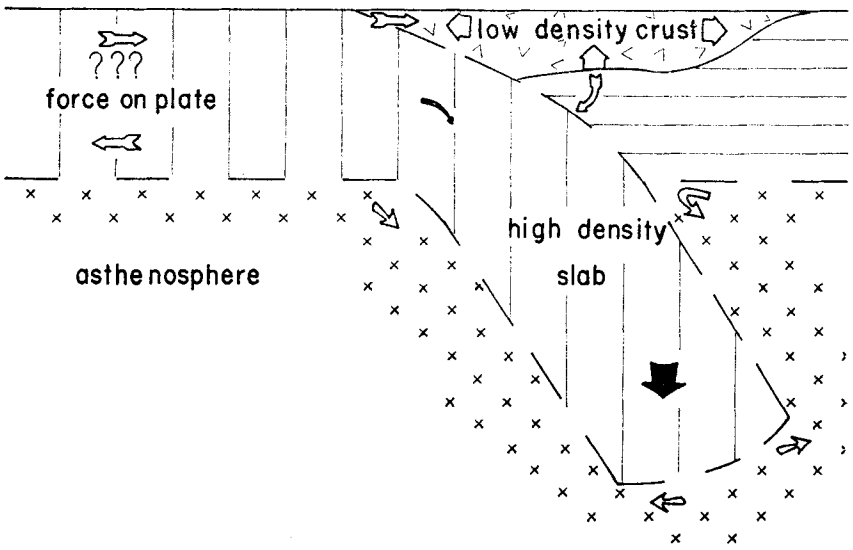

FIG. 1. Schematic diagram shows regions of subduction which affect the flow pattern. Excess density causes the slab to sink. The crust of the island arc tends to spread and rise because of its low density and is also deformed by contact with the slab. Induced flow is set up in the asthenosphere and possibly in the lithosphere beneath the island arc. The slab transmits an unknown force to the oceanic plate. The flow pattern is the result of driving forces (density and force on oceanic plates) and the spatial distribution of rheological properties.

perature on previous convection is thus defined. This procedure is not strongly dependent on the physical parameters in the thermal model or to whether the trajectory of the slab differed somewhat from its dip. Thermal conductivity can redistribute heat over short distances, but the total amount of heat and therefore the net mass anomaly is conserved. (Thermal models which consider the regions surrounding the slab to be isothermal (McKenzie 1969, 1972; Griggs 1972) should not be used in convection or gravity calculations because heat and thus the net mass anomaly is not conserved at the artificial isothermal boundary with the surrounding mantle.)

Neither the ambient thermal gradient before subduction or the coefficient of thermal expansion is known to a high decrease of accuracy. In a numerical model these parameters can be traded off against each other and a simple multiplicative change in the excess density associated with the slab can be easily accommodated by rescaling as explained later. A thermal model based on the seismic velocity structure of the Aleutian slab (modified from Sleep 1973) was used to compute density and viscosity. The volume coefficient of thermal expansion was arbitrarily assumed to be 3×10^{-5} °C^{-1} to get initially a slab density anomaly similar to that used by Grow (1973) and Toksöz *et al.* (1971), although rescaling to a larger value of this coefficient was necessary to fit observed topography and gravity.

The thickness and extent of low density crust below Amchitka is uncertain. Some seismic refraction profiles exist (Shor 1964), but are poorly distributed and would be of little help anyway, since blind use of seismic profiles often creates spurious density anomalies of over 100 mgal. (Emery *et al.* 1970). Travel-time anomalies from the Amchitka explosions to nearby islands (Carder *et al.* 1967) and surface wave velocities (Jacob & Hamado 1972), cannot be easily interpreted since both the slab and the crust affect the result. The best data appears to result from study of local earthquakes near Amchitka. A depth to the Moho of about 38-km results (Kisslinger & Engdahl

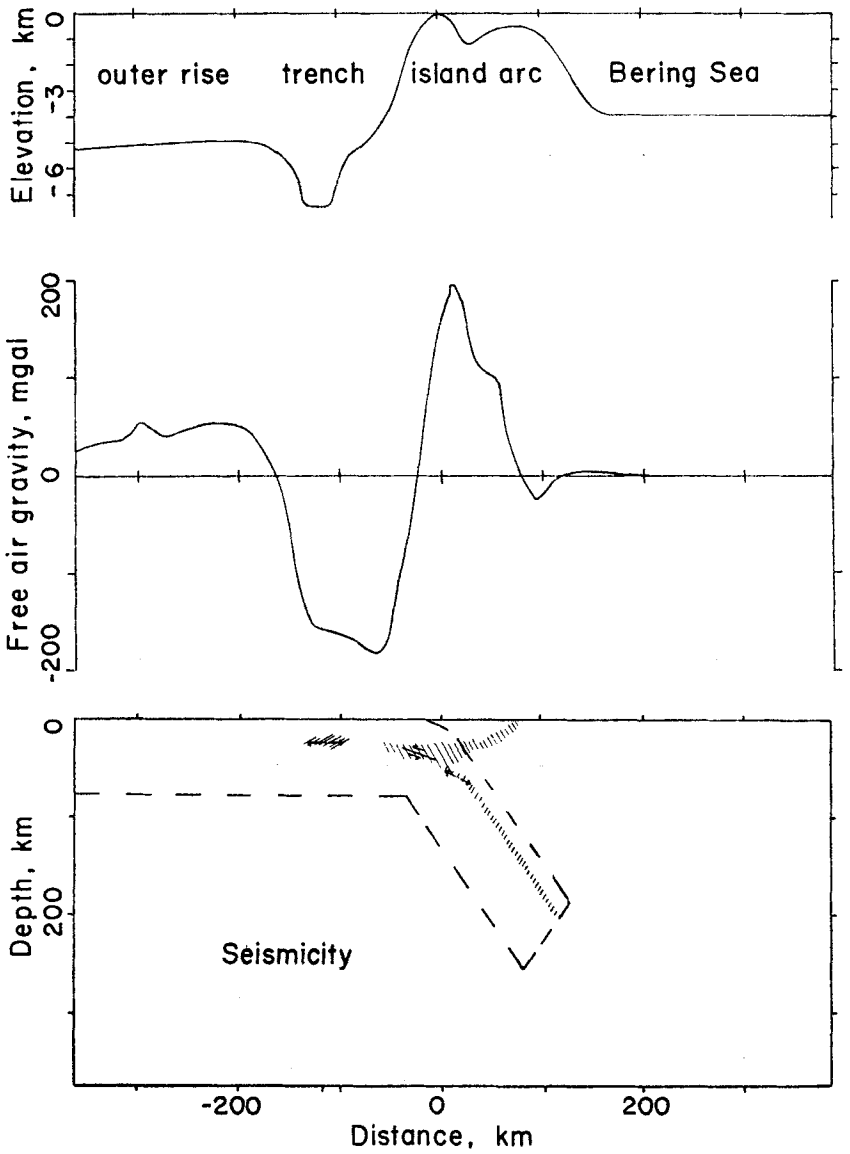

FIG. 2. Observations which are relevant to convective models of the Aleutian arc: topographic provinces (top) near Amchitka (Engdahl 1973); gravity (middle) near Adak (Grow 1973): and seismicity (bottom) relative to slab (Engdahl 1973; Stauder 1972; Sleep 1973). The sedimentary fill which causes the shallow depth the Bering Sea was not included in the models. The zero point is the LONGSHOT explosion site (51° 26′N, 179° 10′E) for all figures herein.

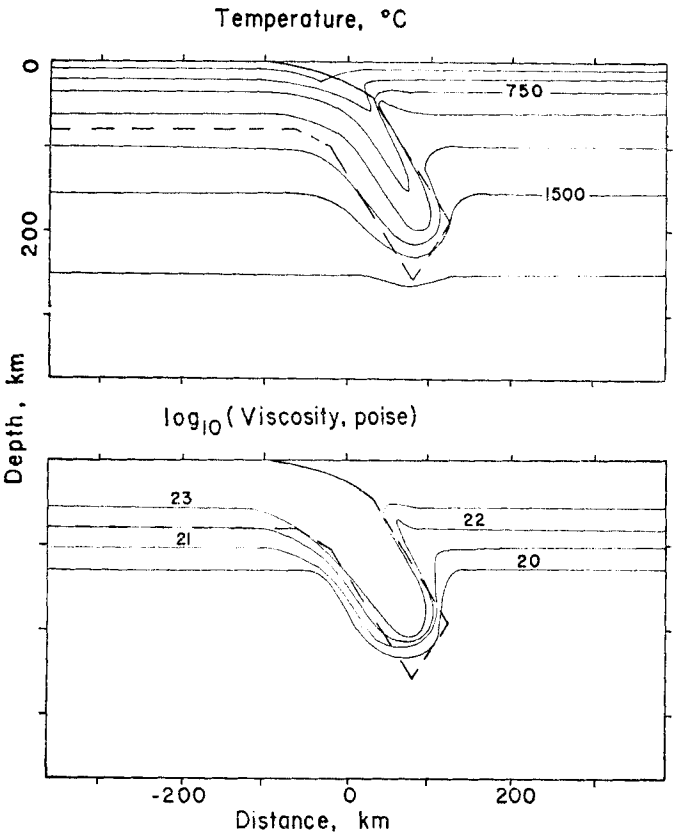

FIG. 3. Computed temperature and viscosity models of slabs were determined from theoretical considerations (Toksöz *et al.* 1973). Density and viscosity were calculated from the assumed temperature. The dip of the slab is 57° and the subduction rate is 4·5 cm/yr. The model has been modified from Sleep (1973) so that the position of the slab seaward of the arc is compatible with the distribution of shallow seismicity (Fig. 2, bottom).

1973). The data used to locate the down-going part of the slab has little sensitivity to the lateral distribution of the crust. The density contrast between crust and mantle was assigned to obtain compatibility with the assumed slab density. A crust–mantle interface based on the gradually dipping slab was assumed in the calculations rather than an interface based on Grow (1973) (Fig. 4).

Low density crust must be explicitly included in the domain of a convection model rather than being added subsequently to the computed topography and gravity anomalies assuming isostasy since the equilibrium position of the crust is not necessarily that deduced from isostasy (Artyushkov 1973, 1974) and since the presence of the crust affects the flow pattern.

A zone of high temperatures beneath the region of active volcanoes (about +80 km in Fig. 2), is indicated by seismic wave attenuation (Grow & Qamar 1973) but the extent of the zone was inferred mainly from gravity and is therefore suspect. Such a zone was not included in the density models.

The topography and gravity profiles calculated from our convection models are compared below with the observed.

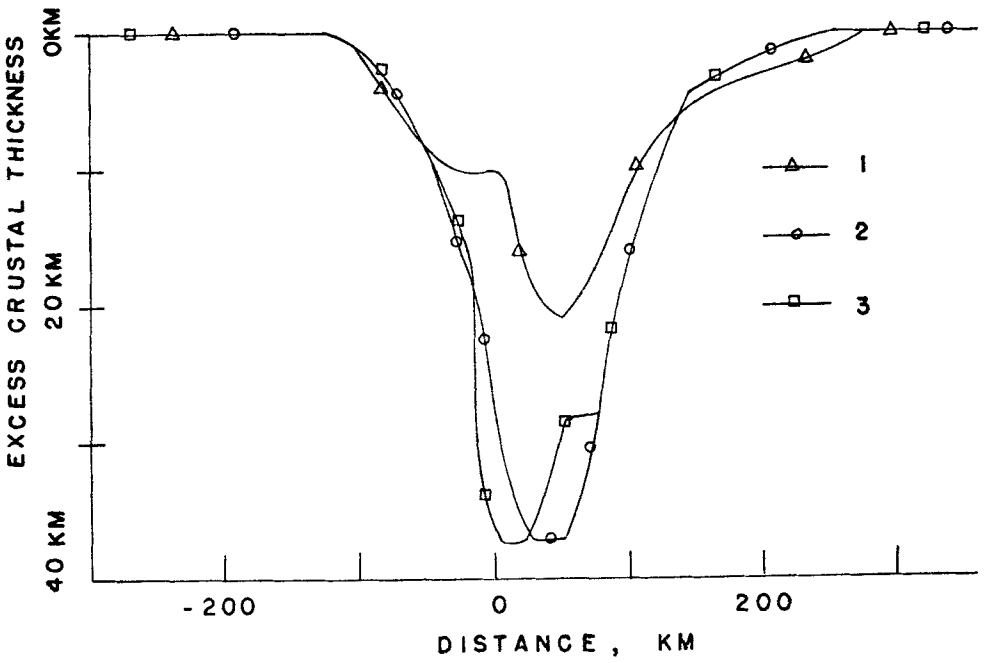

FIG. 4. Lateral distribution of excess (relative to oceanic lithosphere) continental crust used in the numerical models. Curve 1 based on gravity interpretations for an assumed slab density (Grow 1973) is shown for reference. Curves 2 and 3 are compatible with the assumed position of the slab in Fig. 3. Curve 2 was modified to obtain the improved calculated topography given by curve 3.

Stress distribution

Intermediate-depth, shallow thrusting, and shallow normal faulting earthquakes have been observed in the Aleutian area (Fig. 2).

Stress drop for the largest normal and thrust faulting earthquakes in the central Aleutians is about 30 bars (Abe 1972; Wu & Kanamori 1973). Shallow and intermediate earthquakes generally have similar values in other subduction zones (Molnar & Wyss 1972; Wyss & Molnar 1972). A minimum estimate for the shear stress is given by this quantity and shear stress could conceivably be much higher.

Intermediate-depth earthquake mechanism for short slabs are generally tensile along the dip of slab and indicate that the slab is sinking under its own weight and resisted from above (Isacks & Molnar 1971; Smith & Toksöz 1972). Two earthquakes (1963 Jan. 1 and 1965 July 2) in the Aleutians have this type of mechanism but both are shallower than 75 km (Isacks & Molnar 1971). Other intermediate-depth earthquakes are the result of out of plane forces related to the curvature of the arc (Isacks & Molnar 1971; Stauder 1968a, b, 1972). In the absence of contrary data it may be presumed that the down dip tension continues throughout the intermediate-depth earthquake zone.

Shallow thrusting earthquakes which occur above the more horizontal part of the slab are compatible with the kinematics of subduction. These events are often very large. The shallow earthquake zone extends into the lithosphere of the island arc, but no earthquake solutions are available from the Aleutians, although an event in an analogous position beneath Tonga (1965 July 21) was determined to be thrust faulting

(see Appendix B). The intermediate and shallow earthquake zones are continuous with each other.

Normal faulting earthquakes which occur near the seaward wall of the Aleutian trench have generally been attributed to flexure as the slab starts to descend (Stauder 1968a, b; Hanks 1971; Johnson & Molnar 1972). However the depths of these earthquakes as reported by ISC are as great as 50 km and thus occur in the centre of the slab. (Flexure in the normal sense of the word would cause tension in the upper part of the slab and compression in the lower part). The earthquake of 1965 March 30, may have produced a normal fault which extended through the plate (Abe 1972). Examination of seismograms showed that the earthquake of 1966 June 2 produced depth phases indicative of a depth of 46 km (see Appendix B). Aftershocks of the earthquake of 1970 February 27 were located at about 30 km depth by the Amchitka seismograph net (Engdahl 1973, private communication).

The vertical component of stress (f_{yy}, equation (A3b)) near the surface is directly given by the elevation. The oceanic trench and the outer rise (Fig. 2) have both been attributed to dynamic forces associated with convection (Morgan 1965a, b; Elsasser 1967; Walcott 1970; Hanks 1971). The elevation for the island arc is mainly due to isostatic compensation, which in the numerical scheme used is automatically included as a hydrodynamic force acting on the free surface resulting from the low density of the crust. The relative importance of these features can be seen when it is noted that the Aleutian island arc extends 5500 metres above local sea depth, while the trench is depressed 1500 m and the outer rise elevated about 500 m. If the island arc is in part created by horizontal compression of sediments or other low density material, the requirement that the horizontal compressive stress from subduction exceeded the horizontal tensile stress from the tendency of the low density crust to spread provides an important constraint on theoretical models.

Viscosity and rheology

Direct observations constraining the rheological behaviour of the lithosphere, the slab, and the surrounding asthenosphere provide only uncertain constraints. As no data from the Aleutians themselves have been analysed, the data from other regions are reviewed.

The viscosity of the material in the wedge above the slab was determined to be about 5×10^{19} poise from post-seismic rebound in Japan (Nur & Mavko 1974) and about 3×10^{21} poise (apparently given incorrectly as stokes in the abstract) from deformed Pleistocene reefs in New Guinea (Chappell 1974). The former estimate directly provides a minimum estimate, as the long term viscosity cannot be lower than whatever mechanism caused the creep. A maximum value of long term viscosity of about 10^{21} poise can be obtained by noting that even if a transient mechanism caused the post-seismic rebound over an interval of about five years, the transient mechanism must itself relax before the next major earthquake (about 100 years). Otherwise, repeated movements of the slab in the same direction would saturate the transient mechanism precluding it from further stress release.

The viscosity of the oceanic and also the continental lithosphere has been determined to be between 10^{24} and 10^{25} poise from the flexural response to long term loads (Walcott 1970). Studies now in progress of the sedimentation pattern of mid-continent basins and Atlantic continental margins by Walcott & Foucher (1973, private communication), and by us, tend to confirm this result. However, this high a linear viscosity cannot be the rheology of the lithosphere and the slab where they are in contact since subduction at observed rates would be precluded, as the calculations below confirm. A non-linear rheology of some type therefore probably prevails in the highly stressed region although just what parameters should be used is not obvious.

A temperature and depth dependent formula was used to compute linear viscosity

$$\eta = HT \exp \frac{E+kz}{T} \tag{1}$$

η viscosity,

H multiplicative constant, 115. poise/°K

T absolute temperature from thermal model,

E constant related to activation energy of creep, $5{\cdot}22 \times 10^4$ °K,

k constant from depth dependence, $3{\cdot}5 \times 10^{-4}$ °K/cm,

z depth.

These values were chosen to give a gradual transition between the lithosphere and asthenosphere. A different choice of initial geotherm before subduction could be traded off with these constants and the coefficient of thermal expansion to form an identical distribution of excess density and viscosity. For mainly numerical reasons the viscosity of the asthenosphere was restricted to a minimum of 10^{20} poise and the viscosity of the slab and lithosphere to a somewhat too low maximum value of 10^{23} (Fig. 3). This range is large enough that most of the resistance to flow occurs in the slab.

To model the non-linear behaviour of the lithosphere at high stresses and strain rates a visco-plastic rheology was assumed. At low strain rates, such that the total shear stress* computed using the linear viscosity in Fig. 3 was less than some *yield stress*, strain rate was assumed to be proportional to total shear stress and given by this linear viscosity. At higher strain rates total shear stress was assumed to be equal to the yield stress and independent of strain rate. Mathematically this corresponds to using as an apparent viscosity equal to the ratio of yield stress over strain rate in the linear equation for viscous flow (equation (A8)). By using total shear stress we obtain an equation which is invariant to co-ordinate system.

A more complicated non-linear rheology was not used because we wished to permit rescaling and to avoid numerical problems. The use of a somewhat too low maximum for linear viscosity of 10^{23} poise for the lithosphere reduced the computation time needed to obtain solutions good in both the lightly and highly stressed regions, but was large enough that a substantial difference remained between the apparent viscosity of highly stressed regions and the initially assumed linear viscosity.

Fortunately this rheological scheme permits rescaling of results which differ from the observed values by a simple multiplicative constant. Both the velocity field and the stress field can be rescaled independently.

(1) The surface elevation, stress, and gravity anomalies can be doubled by doubling the density, the viscosity and the yield stress. This leaves the velocity field constant.

(2) The velocity can be doubled by halving the viscosity and leaving yield stress and density constant. The stress field, the surface elevation and the gravity anomalies are unaffected.

Length did not need to be rescaled as the region represented by the models was the proper size. Conversely, it can be seen from (2) that in a problem where local density anomalies cause the flow, the magnitude of the highest stress is relatively independent of the viscosity.

Another complication that might be important is that the rheological properties of the material in the fault plane between the adjacent lithosphere may be different from elsewhere in the lithosphere and slab. Limited experimental evidence on blue-

* Shear stress computed on a plane at 45° to the principal axes of stress or equivalently the maximum value of shear stress computed on any plane. Defined mathematically in equation (A12).

schist facies rocks which are believed to be subducted oceanic sediments indicates that such rocks can support little stress even on laboratory time scales (Brace, Ernst & Kallberg 1970). Sediments and deformed sediments are abundant in and landward of the trench and may extend to several kilometres depth (Marlow *et al.* 1973). The possibility that a weak region exists above the slab as it starts down is supported by the observation that shallow thrust faulting zone does not extend above 30 km (Engdahl 1973). Analysis of Love waves and aftershocks produced by the CANNIKIN explosion indicates that the crust of the Aleutian arc has little strength and is weakly stressed in tension normal to the arc (Toksöz & Kehrer 1972; Engdahl 1972).

The material in the wedge between the slab and the lithosphere of the island arc may be continually replaced by induced flow from below (McKenzie 1969; Sleep & Toksöz 1971; Andrews & Sleep 1974). If this flow did not occur heat loss into the slab would reduce temperatures in the wedge, as in the thermal model in Fig. 3. The importance of a low viscosity wedge above the slab is examined below.

Calculations

For purposes of calculation certain assumptions normally made in mantle convection studies were adopted.

(1) Inertia and coriolis forces were ignored since they were many orders of magnitude smaller than viscous forces.

(2) The curvature of the Earth and increasing density material with increasing depth were ignored.

(3) The material was assumed incompressible with respect to hydrodynamic forces.

(4) The free surface of the Earth was modelled as a vertically immovable, horizontally frictionless boundary and the inferred elevation of the surface computed from the vertical stress on that boundary.

These assumptions are discussed by Richter (1973). Basically the last three assumptions contribute mainly geometrical distortion of the computed versus the actual flow field but do not significantly affect the dynamics. The equations for instantaneous convection in a variable viscosity medium and the finite difference method based on Andrews (1972) for solving them are given in Appendix A.

It is necessary to impose artificial boundary conditions around the numerically modelled region to simulate the interaction of the slab with the rest of the mantle, as the entire Earth could not be tractably modelled. At a minimum, these artificial boundary conditions must not produce large spurious velocities and stresses. For example, specification of velocity boundary conditions and a fixed viscosity may result in calculation of extreme values for stress. The oceanic lithosphere must be able to flow into the domain of the model and the asthenospheric material displaced by the slab must be able to flow out. At the surface of the Earth a natural boundary condition —frictionless or free-slip flow parallel to boundary—is evident. The other boundaries represent artificial lines in the Earth where the actual flow field is unknown.

The arbitrarily assumed boundary conditions at the other three boundaries were parallel flow free-slip at the landward boundary and perpendicular flow and zero third derivative of the stream function perpendicular to the boundary on the bottom and sea-ward boundaries. These conditions preclude a net transfer of work between the modelled region and the outside (see Appendix A). This is a reasonable neutral assumption for most of the Earth models, since it is not known whether the slab does work on the return flow and the oceanic plate or vice versa. Simple perpendicular and parallel flow conditions can be justified mainly because the direction of flow is

unknown away from the lithosphere and slab. A more complex boundary condition would only hide this uncertainty.

The need to use artificial boundary conditions limits to some extent what can be learned from numerical models. Clearly, little information is obtained where the flow in the asthenosphere crosses the boundaries. However, as most of the excess density and resistance to flow in our models is concentrated in the slab and the lithosphere, the choice of boundary conditions* for the asthenosphere does not strongly affect the computed streamlines and stress within the slab, nor the computed topography and gravity. For example, the ratio of stresses in the asthenosphere to stresses in the slab was less than 5 per cent in all models.

Some resistance to flow does, however, occur in the asthenosphere and it is also possible that our estimate of the asthenospheric viscosity is in error. Some computed parameters, including long wavelength topographic variations resulting from transfer of force through the asthenosphere to the surface from the slab, are strongly affected by the asthenospheric viscosity and thus uncertain. For the most part interpretations and conclusions from the models are based on parameters which depend on stress transmission through the lithosphere and the slab. Once this part of the flow is understood more subtle effects involving the asthenosphere can be studied.

A 25 km, square grid (32×16) was used for the remainder of the calculations, as a significantly more dense grid would have either greatly increased computation time and exceeded the single precision numerical accuracy of one of the machines used or necessitated bringing the artificial boundaries too near the region of interest. Fine scale features such as individual folds, therefore, could not be resolved. It was also difficult to construct detailed models including distinct rheologies of the fault plane and the crust of the island arc.

The computational strategy adopted in this paper was to introduce complications one at a time so their effect could be appraised and later seek a well-fitting model. Rather simple rheological models were assumed because as the parameters for complex models are not known, the additional complexity would only produce confusion. Apparently reasonable models which yield ridiculous results are of interest at this primitive stage of understanding since they place constraints on the physical parameters of the Earth. Theoretical values of shear stress, elevation, and velocity field were calculated for the numerical models. Gravity anomalies were computed by adding the attractions of the computed elevation and the masses of depth. The results are discussed below.

Results

Twenty-one models of slabs with different rheological assumptions were computed. The position of the density and temperature anomalies were not varied, because the location of the slab is known much more accurately than its rheology. The thickness of low density crust in the island arc was varied once to improve the fit to observed topography and to confirm the insensitivity of other results to that parameter. Two models in which the slab was assumed to subduct at a given rate were also computed to appraise the effect of interaction between the lithospheric plate and the subduction zone.

Computed topography and gravity are plotted in Fig. 5. The streamlines and stress fields for selected models are plotted in Figs 6–10. The parameters used for the various models are tabulated in Table 1 along with the values of selected computed parameters.

* Model 20 was recalculated assuming parallel flow free-slip boundary conditions for the bottom boundary. Stress in the asthenosphere increased from about 2 bars to about 5 bars, and the subduction rate decreased 14 per cent and the depth of the trench 4 per cent. Stresses varied less than 10 bars and stress angles less than 3 degrees at the bottom of the slab.

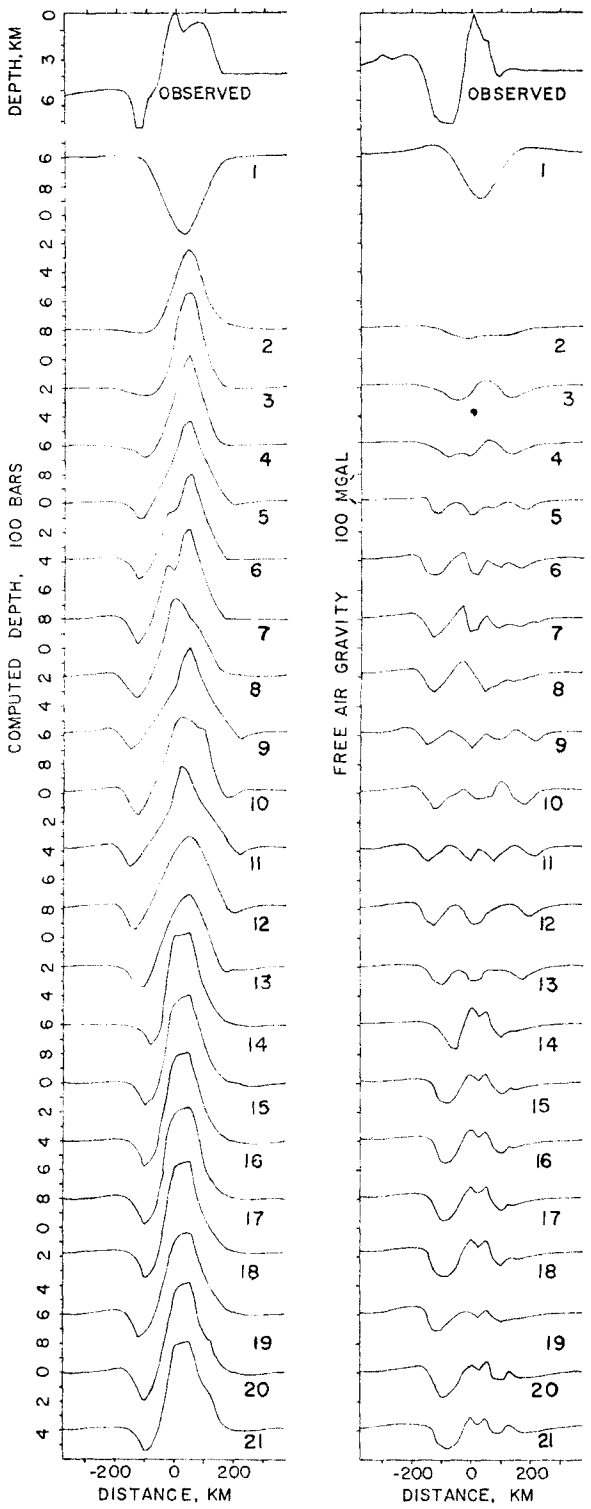

FIG. 5. Computed and observed gravity and topography result from the numerical slab models are plotted as a function of position. The parameters for these models are given in Table 1. Topography was computed as f_{yy} (equation (A3b)) and is hence given in bars. The tick marks on the gravity scale are spaced at 100-mgal intervals.

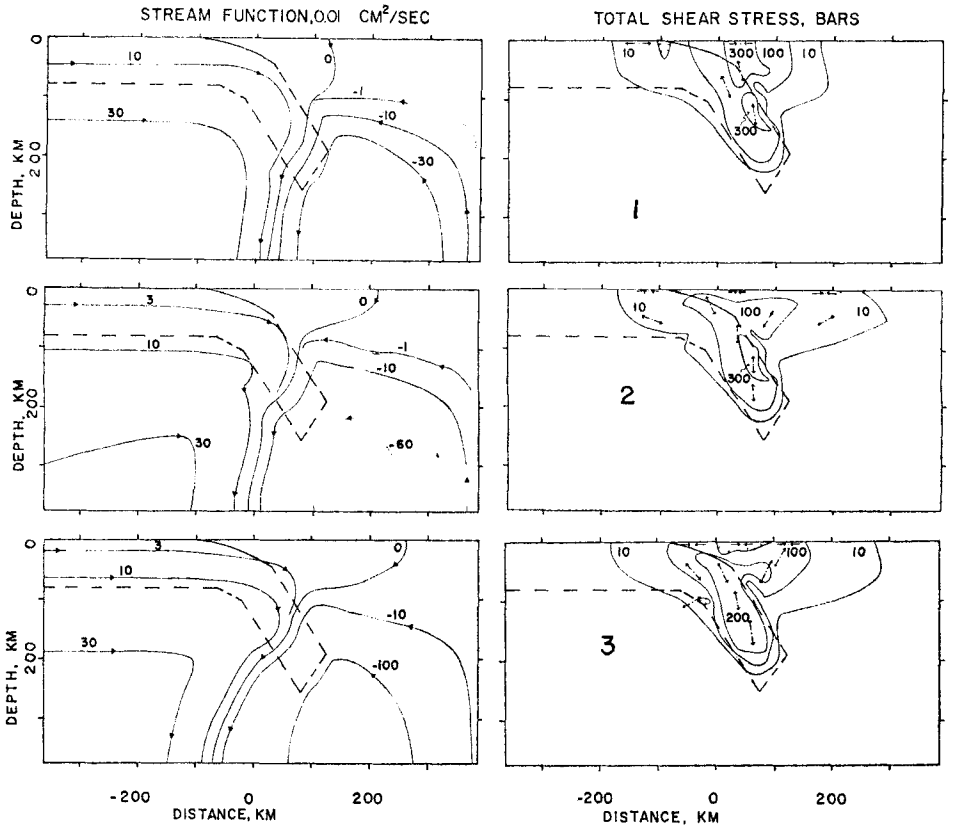

FIG. 6. Stream function (defined in equation (A1)) and shear stress (defined in equation (A12)) are plotted as a function of position for models 1, 2 and 3. Axes of minimum or least compression are denoted by diverging arrows and maximum compression by converging arrows. Velocities are highest where the streamlines closely spaced. The parameters used for calculating models are given in Table 1.

The simplest computed model (1, Fig. 6 top) included no continental crust and assumed a linear viscosity. The streamlines and stress distribution are not compatible with observations (Fig. 2) as the greatest stress is concentrated landward of the shallow thrusting earthquake and as the deep part of the slab is moving much faster than the horizontal plate. The gravity and topography anomalies associated with this slab consist of large single troughs at the position of the island arc. Only the zone of tension seaward of the arc and the stress field at depth in the slab have any resemblance to observations.

Although the need to include the low density continental crust of the island arc in the models should be evident, this model is useful for illustrating defects which plague some of the more complicated models.

1. A zone of negative gravity anomalies occurs directly over the slab, contrary to the observed high in the island arc. In the absence of heterogeneities, force on the surface from excess density in the slab will be concentrated directly above the slab. The observed region of low gravity anomalies, however, is in the trench a considerable distance seaward. The models constructed below examine what heterogeneities are necessary for this effect.

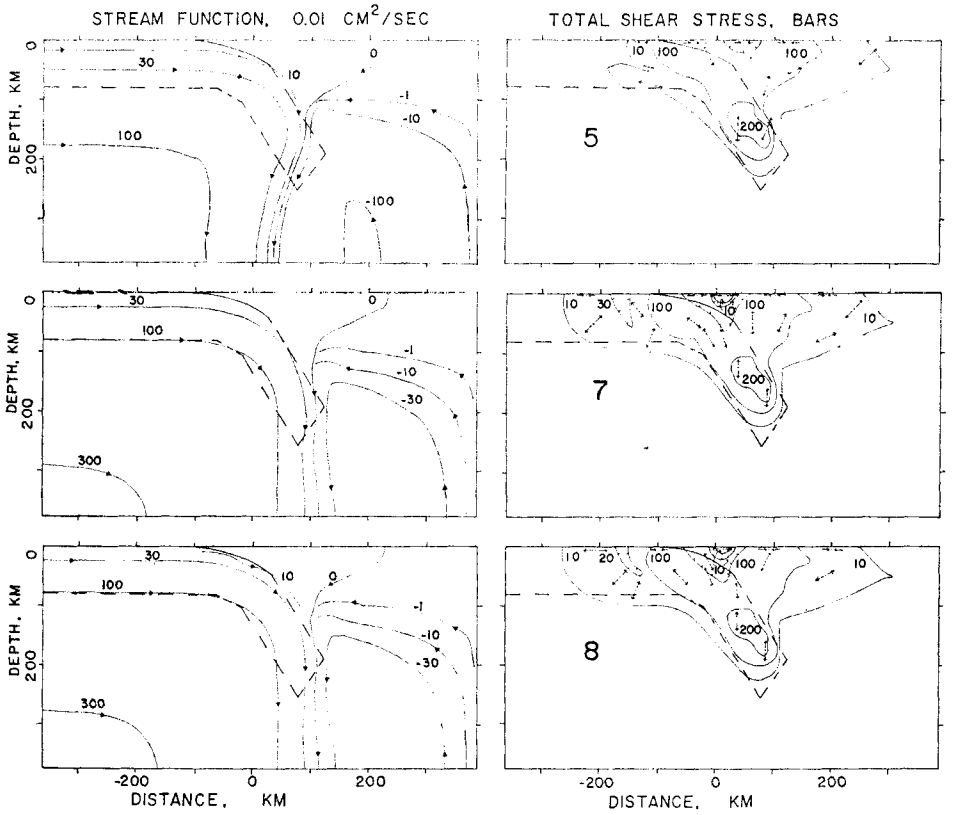

FIG. 7. Stream function and shear stress for models 5, 7 and 8 were calculated from the parameters in Table 1. The region of low stress in models 7 and 8 extending about 25 km in from the fault plane was assumed to have a low viscosity (10^{21} poise). The low stresses farther inland are due to the tendency of the low-density crust to spread.

2. The streamlines in the lower part of the slab cut across the slab from top down with much faster velocity than the horizontal subduction rate. The form of the streamlines can be understood by noting that the slab is supported from above and that excess density causes downward force with a component perpendicular to the slab. The slab as it detaches thus tends to pivot about the point where it is attached to the lithosphere. The rapid detachment of the slab implied by this model is not compatible with the assumed existence of the slab.

Inclusion of a low density continental crust (Fig. 4, number 2) produces positive elevation over the island arc, but a small negative gravity anomaly remains (Fig. 5). No outer rise and only small trench are present. The subduction rate in this model (2, Fig. 6, middle) is much slower than in the model (1) with no crust since the tendency of the low density crust to rise and spread resists subduction which would compact and drag it. The flow rate of the lower part of the slab is again much faster than that of the horizontal plate.

A series of non-linear models using crustal density model number two (Fig. 4) were calculated. Starting with the linear model (2) the computed trench becomes a more prominent feature as the yield stress is decreased to 200 bars (model 3, Fig. 6, bottom) 150 bars (model 4, not illustrated) and 100 bars (model 5, Fig. 7, top) at the

Table 1

Model number	Figure	Crust[1]	Input parameters: Low viscosity regions arc-fault[2]	wedge[3]	Yield stress bars	Gradient bar/km	Rate cm/yr	Output parameters[7]: Elevation[4], bars arc	trench	outer rise	Stress, bars arc	outer rise	Gravity, mgal[5] arc	trench	outer rise
1	6	0	—	No	∞	—	0·68	—	−534	12	—	−19	—	−145	39
2	6	2	—	No	∞	—	0·32	541	−25	—	28	—	−20	−5	—
3	6	2	—	No	200	0	0·51	659	−54	—	29	—	29	−45	—
4	—	2	—	No	150	0·5	0·70	625	−77	0	51	−2	15	−41	10
5	7	2	—	No	100	1·0	1·85	565	−108	6	15	−7	−9	−36	16
6	—	2	F 3×10^{21}	No	100	1·0	2·48	598	−134	13	−41	−19	4	−45	19
7	7	2	F 1×10^{21}	No	100	1·0	4·03	620	−154	21	−93	−32	13	−57	22
8	7	3	F 1×10^{21}	No	100	1·0	4·17	526	−161	21	−74	−33	20	−56	23
9	—	2	—	No	50	1·5	6·75	600	−110	27	−50	−37	7	−30	26
10	8	3	A 1×10^{21}	No	100	1·0	6·75	515	−152	26	−13	−38	−17	−51	27
11	8	3	—	No	50	1·5	7·68	567	−117	28	−50	−39	6	−31	29
12	8	3	—	Yes	100	1·0	7·88	490	−157	25	100	−36	0	−51	27
13	—	3	—	Yes	150	0·5	2·78	511	−137	4	150	−1	−7	−58	12
14	9	3	S 3×10^{21}	Yes	200	0·5	1·54	644	−134	1	17	−2	60	−83	12
15	—	3	S 3×10^{21}	Yes	150	1·0	2·61	611	−148	9	28	−13	34	−67	15
16	9	3	S 1×10^{21}	Yes	150	1·0	3·17	615	−170	10	10	−21	43	−73	18
17	9	3	L 1×10^{21}	Yes	150	1·0	4·21	636	−177	21	12	−30	45	−75	21
18	10	3	L 1×10^{21}	Yes	150	1·0	3·17[6]	630	−172	13	10	−32	54	−61	29
19	10	3	S 1×10^{21}	Yes	100	1·5	5·86	567	−157	30	13	−40	16	−57	24
20	10	3	L 1×10^{21}	Large	150	1·0	6·68	625	−194	28	22	−42	31	−82	24
21	—	3	L 1×10^{21}	Large	150	1·0	3·17[6]	606	−148	10	12	−51	51	−58	29

[1] See Fig. 4; 0 indicates no crust assumed; density contrast is 0·3 g cm^{-3}.
[2] Viscosity in poise; F, fault plane; A, entire arc; S, front arc; L, largest area of front arc.
[3] Viscosity is 10^{20} poise.
[4] Zero is right-hand boundary.
[5] Arbitrary zero.
[6] Assumed velocity boundary condition.
[7] Extreme values not necessarily in same location: omitted if feature not present in results.

surface. In the latter two models and several subsequent ones, the yield stress was assumed to increase with depth, so that the tendency for the slab to detach was decreased. The subduction rate increased as the yield stress was reduced (Table 1). The region of maximum stress in the model (3) with a yield stress of 200 bars, which generally defines the region of maximum strain rate in later models, is in general agreement with the distribution of earthquakes (Fig. 3, bottom). It should be noted that although a minimum of computed stress exists beneath the island arc near the surface, the stress is compressional in contrast with other models below.

Three approaches were made to construct models with more rapid flow rates in which the slab did not detach. First, it was assumed that the region near the upper part of the fault between the slab and the arc had less resistance to deformation. Although this was done numerically by imposing a low linear viscosity on that region, the results can also be interpreted as being due to a reduced yield stress equal to that stress which was computed. For the first model (6) of this type a stress of about 60 bars resulted from an assumed linear viscosity of 3×10^{21} poise near the fault (not illustrated). The tendency for the slab to detach in this model still exists, but the crust of the arc is weakly in tension. By reducing the viscosity of the fault plane to 10^{21} poise and the corresponding stress to 30 bars in model (7) the tendency of the slab to detach is removed (Fig. 7, middle). The increased prominence of the trench, the outer

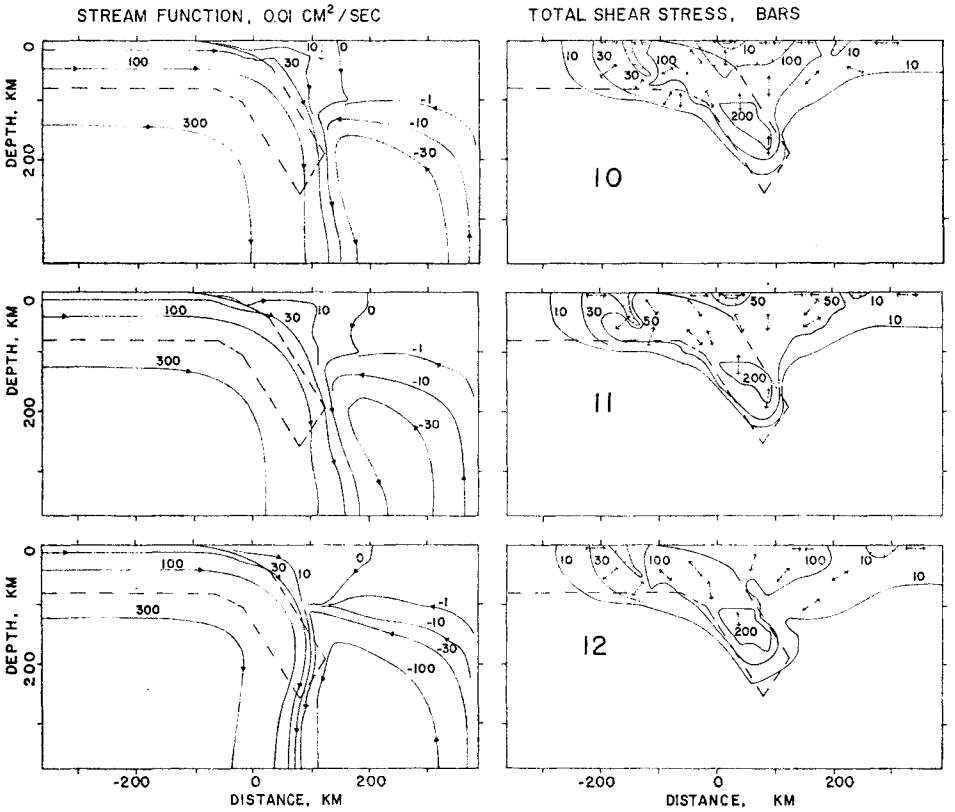

FIG. 8. Stream function and shear stress for models 10, 11 and 12 were calculated from the parameters in Table 1. The region of low shear stress in the island arc in model 14 was assumed to have a viscosity of 1×10^{21} poise. The low viscosity (10^{20} poise) wedge in models 12–19 is best indicated by the indentation of the 10-bar contour above the slab in model 14 (Fig. 9, top).

rise, and the zone of tension seaward of the trench axis in model (7) should be noted (Fig. 5).

This latter model provided a good enough fit to observations of stress and topography seaward of the arc, that a model (8, Fig. 7, bottom), with new crustal thickness distribution (Fig. 4, Number 3) was computed to improve the fit of the topography to observations. The peak of the island arc now occurs in the right place although a complete match is not yet obtained (Fig. 5). No further modifications of the assumed crustal structure were made because this minor modification to improve topography did not greatly alter computed stress, topography seaward of the arc, or gravity (Fig. 5). Detailed fitting to an individual topographic profile could be made after an otherwise satisfactory model is obtained.

It should also be noted at this point that the initial density estimate chosen for the slab based on Grow (1973) is probably too low, since the computed 150 bar (0·65 km) depth* of the trench and the 550 bar (2·43 km) elevation of the arc are about a factor of 2·3 lower than the observed 1·5 km depth and 5·5 km elevation respectively. This would give a not unreasonable density contrast of $0{\cdot}7\ \mathrm{g/cm^{-3}}$ between the crust of the island arc and the mantle and a thermal expansion coefficient of $7\times10^{-5}\ ^{\circ}\mathrm{C}^{-1}$. This coefficient is in general agreement with the values used for modelling the thermal contraction of sea-floor near mid-ocean ridges of about $5\times10^{-5}\ ^{\circ}\mathrm{C}^{-1}$ (Sclater & Francheteau 1970).

The gravity anomaly over the trench in models 7 and 8 is about 50–60 mgal (Fig. 5). Even with rescaling by a factor of 2·3 to fit the topography the gravity anomaly is insufficient to fit the observed 180 mgal. The positive anomaly landward of the trench is also seaward to the frontal arc, the observed position of the high. It is evident in these models that an excess amount of force is still being transmitted directly up from the slab to the surface of the island arc.

Attempting to improve the fit to observation by reducing the yield stress at the surface to 50 bars resulted in reducing the trench depth to 110 bars (0·48 km) (models 9, not illustrated and 11, Fig. 8, middle). The yield stress is exceeded in tension at the centre of the arc in these models. Rapid spreading of the crust produces the kinks in the stream lines. A model (10, Fig. 8, top) assuming that the entire crust of the island arc had a reduced viscosity of 10^{21} poise, resulted in a region of near zero gravity anomalies near the frontal arc. The topography and stress fields of these models are reasonable, despite the poor fit to gravity (Fig. 5).

The remaining models assume that the wedge between the slab and the island arc is occupied by asthenosphere having a viscosity of 10^{20} poise rather than the viscosity in Fig. 3 used above. This modification would be expected to produce faster descent of the slab and to reduce the transmission of force directly up from the slab. Induced flow at normal subduction velocities in the wedge would maintain high temperatures and low viscosity without any intrinsic difference in material properties (Andrews & Sleep 1974).

The first wedge model (12, Fig. 8, bottom), resulted in rapid subduction and large horizontal compressional stresses throughout the island arc. The yield stress in this model is the same as that in the series of previous models, 100 bars at the surface and 1 bar $\mathrm{km^{-1}}$ increase with depth. A trench and outer rise are present as well as a zone of tension seaward of the slab (Fig. 5). The gravity anomaly for this model is too negative landward of the arc. Use of a higher yield stress of 150 bars and a gradient of 0·5 bar $\mathrm{km^{-1}}$ resulted in a moderate subduction rate and detachment of the slab (Model 13, not illustrated). No outer rise is present and the gravity anomaly

* The elevation, f_{yy}, is computed directly as pressure in bars. It must be converted to elevation by dividing by the specific weight of the material forming the topography. A conversion using $2{\cdot}3\times10^{3}$ dyne $\mathrm{cm^{-3}}$, the specific weight of the mantle beneath water, is given to aid comparison with observed data. The density of the island arc is somewhat lower and the computed elevation of the arc increased somewhat.

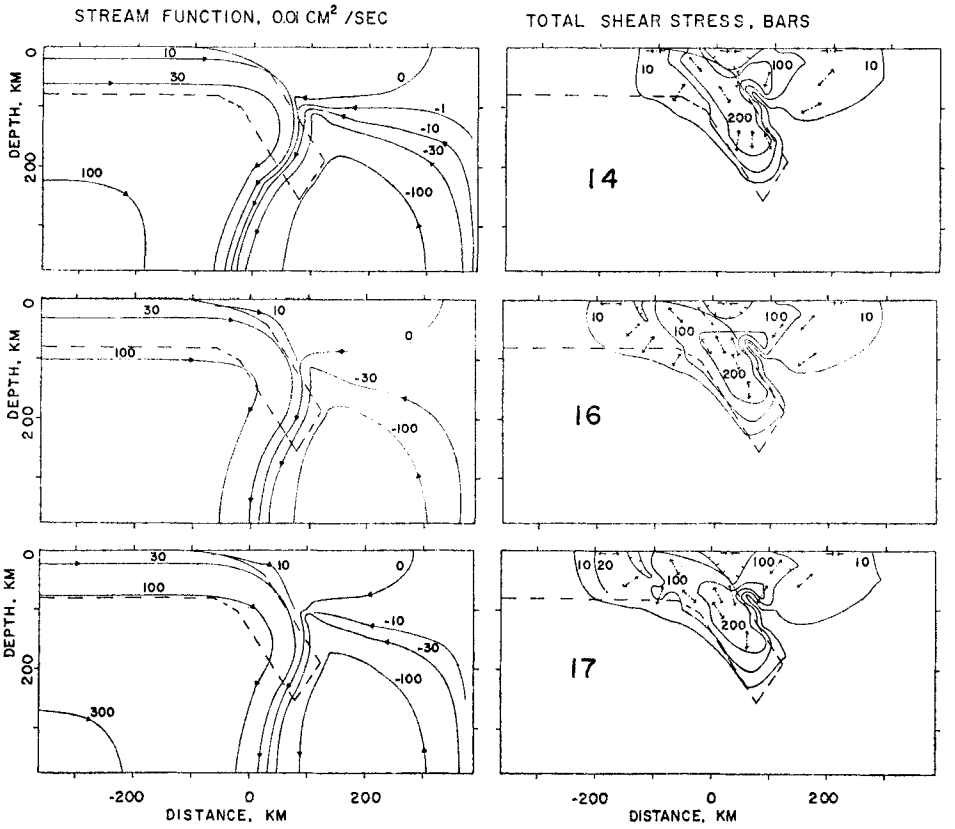

FIG. 9. Streamlines and shear stress for models 14, 16 and 17 were computed from the parameters in Table 1. The low stress region of the frontal arc in these models was assumed to have a low viscosity of 10^{21} poise. The low viscosity wedge in model 12 was also assumed. The frontal arc region in models 17, 18 (Fig. 10, top), 20 (Fig. 10, bottom), and 21 (not illustrated) is somewhat larger than that in models 14, 15 (not illustrated), 16, and 19 (Fig. 10, middle).

is a generally low region over the arc. It is evident from these models that the low viscosity wedge alone cannot preclude transmission of stress upward into the arc.

A series of models including a low viscosity for the crust of the frontal arc were constructed. In the first model (14, Fig. 9, top), a yield stress of 200 bars and a stress gradient of 0·5 bar km^{-1} was assumed. A deep trench which was too close to the island arc resulted (Fig. 5). The gravity anomaly over the arc was strongly positive yet somewhat less than the trench anomaly. Subsequent models resulted in an improved position of the trench, presence of an outer rise and a reduced tendency for the slab to detach, but did not result in increasing the gravity anomaly over the arc.

A variation of the assumed viscosity of the frontal arc from 3×10^{21} poise to 1×10^{21} poise in models 15 (not illustrated) and 16 (Fig. 9, middle), resulted in little change in either the flow pattern or the gravity anomalies. Reduction of the surficial yield stress to 150 bars in these models permitted a larger subduction rate than in model 14. The tendency for the slab to detach and the small amplitude of the outer rise are deficiencies present in these two models. Increasing the size of the low viscosity region in the frontal arc in model 17 (Fig. 9, bottom) results in a slightly larger outer rise than in model 16. A model (19, Fig. 10, middle) having a yield stress

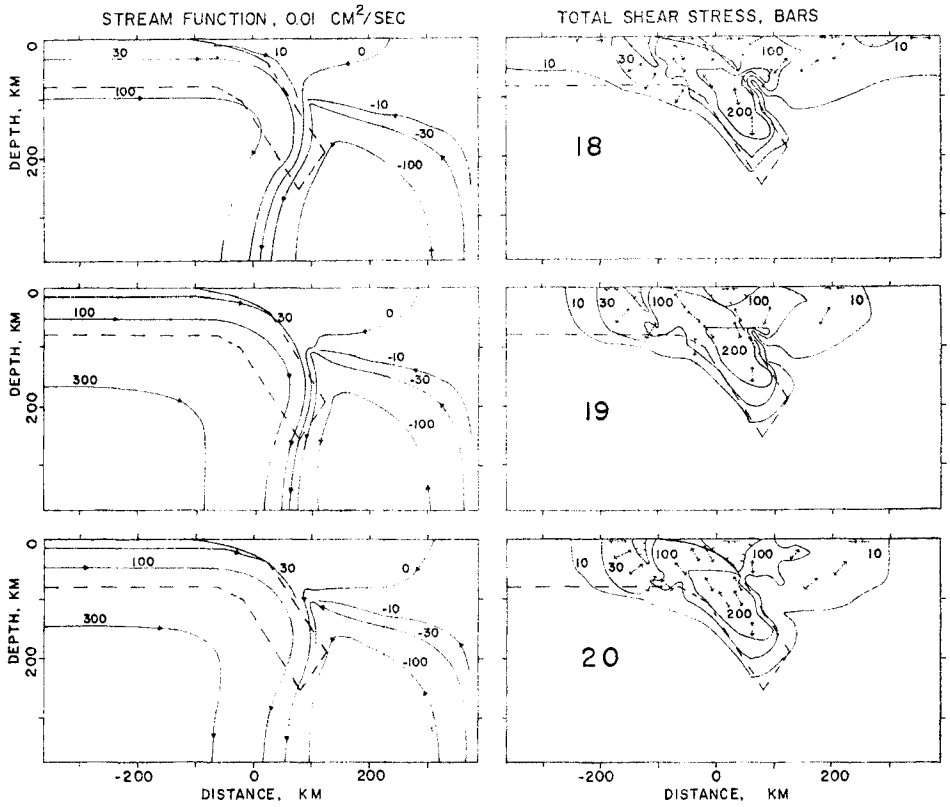

FIG. 10. Streamlines and shear stress for models 18, 19 and 20 were computed from the parameters in Table 1. The top of the low viscosity wedge in models 20 and 21 (not illustrated) is larger than that in the other wedge models. The smaller low viscosity region of frontal arc is assumed in model 18, 20 and 21.

of 100 bars at the surface and the frontal arc rheology of model 16 had a large outer rise and a rapid subduction rate. The amplitude of the gravity anomalies over the frontal arc in model 19 is lower than in the other wedge models (Fig. 5).

Model 20 (Fig. 10, bottom), included a larger low viscosity wedge than the previous models and the large low viscosity wedge of model 17. The 194 bar (0·85 km) amplitude for the trench in model 20 was the largest obtained (Table 1). As with model 19 the computed gravity anomalies in model 20 are lower than in model 17 (Fig. 5).

An additional model 18 (Fig. 10, top) was calculated with parameters identical to model 17 except that the oceanic lithosphere was constrained to move at a reduced rate of 3·17 cm/yr rather than the computed rate of 4·21 cm/yr of model 21. Other than for tensile stress on both sides of the arc no significant modifications of the results were obtained. Constraining model 20 to move at 3·17 cm/yr rather than 6·68 cm/yr resulted in some reduction of the size of the trench and outer rise (Model 21, not illustrated). This confirms that the results are not overly sensitive to the boundary condition used for the oceanic plate.

Further modifications of these models might improve the fit of observed and theoretical gravity anomalies over the arc. Gravity anomalies, which are the differences of attractions from masses at depth and displacements of the free surface from hydrodynamic forces related to the masses, are sensitive to dynamic details. The failure

of the models to have large enough positive anomalies over the frontal arc is due to excessive transfer of force directly up from the slab. With the 25-km grid used, concentration of shear along a narrower fault plane is precluded and the crust of the front arc cannot be modelled separately from the fault plane. Thus an improved model even if obtained would yield little new information. Finer scale models will be necessary to further examine this problem.

Discussion and implications

Although no model was totally successful a general qualitative fit to observations was obtained in several cases. As with any computation, the utility is mainly quantification and ordering of effects which can be qualitatively understood. The results though incomplete are more detailed than previous work and help demarcate future study by eliminating certain classes of models from consideration. The production of such features as the trench and the outer rise in the models gives indication that the hypothesis that these features are produced by hydrodynamic forces is at least physically realizable.

Unfortunately the simplest linear and constant rheology models (1–6) were the least successful. Heterogeneities in the rheology of the island arc and the wedge above the slab were introduced in later models. The latter change is the least fundamental as it could be considered change to a different thermal model. The grid used proved too coarse to accurately represent the crust of the island arc and the fault plane above the slab. Subsequent calculations will need more resolution of those complex regions.

Stress

The stress distribution in many of the models is compatible with seismic results. Tensile stress seaward of the trench, thrust faulting beneath the trench, and tension along the slab were easily obtained. The difficulty in accurately delineating fault plane solutions and the possibility of time-dependent effects related to great earthquakes reduces the power of seismology to eliminate possible models. The models, however, are a good starting point on which to build time-independent or time dependent viscoelastic models (Smith & Toksöz 1972; Nur & Mavko 1973) as the average mechanical properties and stress are defined.

An interesting feature of the models is that the stress near base of the slab is vertical tension. This occurs because resistance from the asthenosphere was small enough that even the mass at the end of the slab caused tension above it. If reliable earthquake mechanism can be obtained in the basal region of a short slab, it appears that the viscosity of the asthenosphere and its resistance on the slab can be deduced. If the subduction rate is faster than the rate at which large detached pieces of lithosphere sink, detachment is impossible. In this case the slab would be under compression, not tension (Isacks & Molnar 1971; Smith & Toksöz 1972). This possibility did not occur in any of the models as the slab was assumed not to penetrate high viscosity material below the asthenosphere. The calculations are of little help in determining this limit as the subduction rate may be varied at will by rescaling.

The stress over the island arc varied from strongly compressive to strongly tensile with the relatively minor changes between models. If tectonic stresses are to pile and accrete an island arc, compression must occur at least during the folding process. The most successful models (17–20) assumed that the crust of the frontal arc had a low viscosity. Models in which the force from the continental crust was strongly transmitted to the oceanic plate had a tendency for the slab to detach. One can thus infer that the crust of the island does not strongly retard plate motions. It may also be inferred that, once the frontal arc is accreted into equilibrium with forces from the slab, subsequent deformation will diminish. Thus continuous subduction may cause apparently episodic deformation.

This implies that a mainly surface process, the supply of sediment to the island arc, may affect the course of a deep tectonic process. The sediment supply to different trenches, for example the Marianna and eastern Aleutian trenches, is highly variable. The composition of sediments, particularly carbonates, has varied throughout geological time (Garrels, Mackenzie & Siever 1972).

Topography and gravity

The computed models did not obtain an excellent fit to observed topography and gravity, but reproduced the principal provinces—arc, trench, and outer rise. Fitting data from the trench can be compared with the theoretical results to obtain a calibration of the density of the slab and thus the stresses in the problem. The crustal structure in the trench is known and the local topographic and gravity anomalies are large reducing the uncertainty of the effects at long wavelength discussed below. It was necessary to assume a slab density of at about a factor of 2 greater than that of Grow (1973) to obtain a reasonable topography for the trench. Calculations of surficial and lithospheric structure of the arc (Grow 1973; Grow & Qamar 1973) could be repeated using this density. The new crustal density distribution then could be reinserted into the dynamical calculations. This exercise was not attempted mainly because an excellent fit to observations was not obtained for gravity anomalies over the arc and because of the coarse grid used in the calculations.

An outer rise was present in those models where the slab was not greatly resisted by the island arc (7–12, 17–21). Steep seaward sides of the trench occur in these models, because with a non-linear rheology a large lateral gradient of stress can exist in the range of stress for linear viscosity without extrapolation to very high stresses. This important feature of non-linear models permits an outer rise in several subsequent models which did not include the 5 kbar stress beneath the arc deduced by Hanks (1971) and Watts & Talwani (1974) from linear calculation. The choice of a low artificial viscosity for the lithosphere and the need to limit the domain of the calculation preclude conclusions based on the detailed shape of the computed rise. Walcott (1970) has already demonstrated that the outer rise is best modelled by flexure in a lithospheric plate having a viscosity of 10^{24} to 10^{25} poise. The viscosity of the most rapidly subducting models computed (9–11) and (20) is about $3—10^{23}$ poise just below the end of this range after rescaling to fit the observed Aleutian subduction rate and topography. It was learned however, that large stresses beneath the island arc were unnecessary for an outer rise to exist.

Long wavelength topographic and gravity anomalies caused by transmission of force from the slab to the surface through the asthenosphere may be superimposed on long wavelength gravity anomalies from the direct attraction of the slab and shorter wavelength topography and gravity anomalies near the arc. Little on this aspect can be learned from the arc models because the long wavelength anomalies were controlled by artificial boundary conditions and an arbitrary asthenosphere viscosity and since elevation is determined by integration of (A6) from an arbitrary value at some point. Some caution in using density models of limited regions particularly the outer rise to determine slab density is warranted, as offsetting of direct gravitational attraction and long wavelength hydrodynamic effects is possible (Watts & Talwani 1974, 1975). Using anomalies with 'regionals' removed to determine slab density is an even more doubtful method.

Mechanism of volcanism

A marked improvement in the models was obtained by including a low viscosity wedge between the slab and the island arc. In the wedge models (13–21), a greater transfer of force from the slab to the trench was obtained as force could not be transmitted directly up through the wedge. Calculations by Andrews & Sleep (1974)

indicated that the descent of the slab would induce sufficient flow in the wedge to maintain high temperatures. For flow to occur the yield stress in the wedge could not be appreciably greater than the yield stress in the slab. Similar mechanical properties of the fault plane immediately above the wedge and the material on either side permitted the slab to entrain material and enlarge the low viscosity wedge at the expense of the lithosphere of the island arc forming a source region for volcanism. Little can be learned from the models of this paper about the details of this ablation process because of the coarseness of the grid used.

As noted already models which permit much force transmission between the slab and the island arc have low gravity anomalies over the frontal arc, lack an outer rise, and have detachment of the slab. This observation tends to refute the hypothesis that frictional heat on the fault plane between the slab and the island arc causes island arc volcanism. The maximum stress in that region in the more successful models (7–12, 17–21), is less than 700 bars (rescaled by a factor of at most 2·5 to fit topography and gravity) in contrast with the minimum of 2000 bars needed for frictional melting (Minear & Toksöz 1970; Toksöz, Minear & Julian 1971; Turcotte & Schubert 1973). More efficient transmission of force to the trench than obtained in the models would imply in less friction on the fault plane. The observation that an outer rise can be obtained without high stresses on the fault plane enervates another argument for large amounts of frictional heating. The only conceivable way to obtain volcanism from frictional heating would be for the slab to be resisted by a small region of high stress due to different mechanical properties. A physical reason for this possibility is not evident.

Future models

One may conclude that the physics of a region as complicated as an island arc can be modelled. This study, as with previous ones, suffers from errors of resolution at short wavelengths and dependence on synthetic boundary conditions at long wavelengths. The results presented above are thus most applicable to intermediate scale features such as arc, trench and outer rise and complementary to larger and smaller scale models. For example, analytic models of flexure of the outer rise (Walcott 1970) give more accurate information on its rheology, but less information on the forces causing the flexure than this paper. Until improved computational methods are found careful use of variously sized model regions will be necessary for efficient appraisal of hypotheses about the dynamics of the Earth.

Acknowledgments

I have had helpful discussions with D. Joe Andrews, E. R. Engdahl, Peter Molnar, Al T. Smith and M. Nafi Toksöz on various aspects of the problem. Sean Solomon critically read the manuscript catching an error and suggesting several improvements.

I thank Northwestern University for providing computer funds. This research was in part supported by the Earth Sciences section of the National Science Foundation, NSF Grant DES 74–22338.

Department of Geological Sciences,
Northwestern University,
Evanston, Illinois 60207.

References

Abe, K., 1972. Lithospheric normal faulting beneath the Aleutian trench, *Phys. Earth Planet. Int.*, **5**, 190–198.

Andrews, D., 1972. Numerical simulation of sea floor spreading, *J. geophys. Res.*, **77,** 6470–6481.

Andrews, D. & Sleep, N., 1974. Numerical modelling of tectonic flow behind island arcs, *Geophys. J. R. astr. Soc.*, **38,** 237–251.

Artyushkov, E., 1973. Stresses in the lithosphere caused by crusted thickness inhomogeneities, *J. geophys. Res.*, **78,** 7675–7708.

Artyushkov, E., 1974. Can the Earth's crust be in a state of isostasy, *J. geophys. Res.*, **79,** 741–752.

Brace, W., Ernst, W. & Kallberg, R., 1970. An experimental study of tectonic overpressure in Franciscan rocks, *Geol. Soc. Amer. Bull.*, **81,** 1325–1338.

Burggraf, O., 1966. Analytical and numerical studies of the structure of steady separated flows, *J. Fluid Mech.*, **24,** 113–151.

Carder, D., Tocher, D., Bufe, C., Stewart, S., Eisler, J. & Berg, E., 1967. Seismic wave arrivals from LONGSHOT, 0 to 27, *Bull. seism. Soc. Am.*, **57,** 573–590.

Chappell, J., 1974. Upper mantle rheology in a tectonic region: evidence from New Guinea, *J. geophys. Res.*, **79,** 390–398.

Elsasser, W., 1967. Convection and stress propagation in the upper mantle, *Princeton Univ. Tech. Rept.* **5,** June 15.

Emery, K., Uchupi, E., Phillips, J., Bowin, C., Bunce, E. & Knot, S., 1970. Continental rise off eastern North America, *Am. Assoc. Petrol. Geol. Bull.*, **54,** 44–108.

Engdahl, E. R., 1972. Seismic effects of the MILROW and CANNIKIN nuclear explosions, *Bull. seism. Soc. Am.*, **62,** 1411–1423.

Engdahl, E. R., 1973. Relocation of intermediate depth earthquakes in the central Aleutians by seismic ray tracing, *Nature Phys. Sci.*, **245,** 23–25

Garrels, R., Mackenzie, F. & Siever, R., 1972. Sedimentary cycling in relation to the history of the continents and oceans, *The Nature of the solid earth,* 93–121, ed. Robertson, McGraw–Hill, New York.

Griggs, D., 1972. The sinking lithosphere and the focal mechanism of deep earthquakes, *The Nature of the Solid earth,* 361–384, ed. Robertson, McGraw–Hill, New York.

Grow, J., 1973. Crustal and upper mantle structure of the central Aleutian arc, *Geol. Soc. Am. Bull.*, **84,** 2169–2192.

Grow, J. & Qamar, A., 1973. Seismic wave attenuation beneath the central Aleutian arc, *Bull. seism. Soc. Am.*, **63,** 2155–2166.

Hanks, T., 1971. The Kuril trench–Hokkaido rise system: large shallow earthquakes and simple models of deformation, *Geophys. J. R. astr. Soc.*, **23,** 173–189.

Herrin, E., 1968. 1968 seismological tables for P phases, *Bull. seism. Soc. Am.*, **58,** 1193.

Isacks, B. & Molnar, P., 1971. Distribution of stresses in the descending lithosphere from a global survey of focal mechanism solutions of mantle earthquakes, *Rev. Geophys. Space Phys.*, **9,** 103–174.

Isacks, B., Sykes, L. & Oliver, J., 1969. Focal mechanisms of deep and shallow earthquakes in the Tonga–Kermedec region and the tectonics of island arcs, *Bull. Geol. Soc. Am.*, **80,** 1443–1470.

Jacob, K., 1972. Global tectonic implications of anomalous seismic P travel times from the nuclear explosion LONGSHOT, *J. geophys. Res.*, **77,** 2556–2573.

Jacob, K. & Hamada, K., 1972. The upper mantle beneath the Aleutian arc from pure-path Rayleigh-wave dispersion data, *Bull. seism. Soc. Am.*, **52,** 1439–1463.

Jacoby, W., 1970. Instability in the upper mantle and global plate movements, *J. geophys. Res.*, **75,** 5671–5680.

Johnson, T. & Molnar, P., 1972. Focal mechanisms and plate tectonics of the southwest Pacific, *J. geophys. Res.*, **77,** 5000–5032.

Kisslinger, C. & Engdahl, E., 1973. Interpretation of the Wadati diagram with relaxed assumptions, Bull. seism. Soc. Am., 63, 1723–1736

Marlow, M., Scholl, D., Buffington, E. & Alpha, T., 1973. Tectonic history of the central Aleutian arc, *Geol. Soc. Am. Bull.*, **84,** 1555–1574.

McKenzie, D., 1969. Speculations on the consequences and causes of plate motions, *Geophys. J. R. astr. Soc.*, **18,** 1–32.

McKenzie, D., 1972. Plate tectonics, *The Nature of the solid earth*, 323–360, McGraw–Hill, New York.

Mendiguren, J., 1971. Focal mechanism of a shock in the middle of the Nazca plate, *J. geophys. Res.*, **76,** 3861–3879.

Minear, J. & Toksöz, N., 1970. Thermal regime of a downgoing slab and new global tectonics, *J. geophys. Res.*, **75,** 1397–1419.

Mitronovas, W., Isacks, B. & Seeber, L., 1969. Earthquake locations and seismic wave propagation in the upper 250 km of the Tonga island arc, *Bull. seism. Soc. Am.*, **59,** 1115–1135.

Molnar, P. & Wyss, M., 1972. Moments, source dimension and stress drops of shallow focus earthquakes in the Tonga–Kermadec arc, *Phy. Earth Planet. Int.* **6,** 263–278.

Morgan, W., 1965a. Gravity anomalies and convection currents, 1, A sphere and cylinder sinking beneath the surface of a viscous fluid, *J. geophys. Res.*, **70,** 6175–6187.

Morgan, W., 1965b. Gravity anomalies and convection currents, 2. The Puerto Rico trench and Mid-Atlantic rise, *J. geophys. Res.*, **70,** 6189–6204

Nur, A. & Mavko, G., 1974. Postseismic viscoelastic rebound, *Science*, **183,** 204–206.

Oxburgh, E. & Turcotte, D., 1970. Thermal structure of island arcs, *Bull. Geol. Soc. Am.*, **81,** 1665–1688.

Oxburgh, E. & Turcotte, D., 1971. Origin of paired metamorphic belts and crustal dilation in island arc regions, *J. geophys. Res.*, **76,** 1315–1327.

Richter, F., 1973. Dynamical models for sea-floor spreading, *Rev. Geophys. Space Phys.*, **11,** 223–287.

Sclater, J. & Francheteau, J., 1970. The implications of terrestrial heat flow observations on current tectonic and geochemical models of the crust and upper mantle of the Earth, *Geophys. J. R. astr. Soc.*, **20,** 493–509.

Shor, G., 1964. Structure of the Bering Sea and the Aleutian Ridge, *Marine Geology*, **1,** 213–219.

Sleep, N., 1973. Teleseismic P-wave transmission through slabs, *Bull. seism. Soc. Am.*, **63,** 1349–1373.

Sleep, N. & Toksöz, N., 1971. Evolution of marginal basins, *Nature*, **233,** 548–550.

Smith, A. & Toksöz, M., 1972. Stress distribution beneath island arcs, *Geophys. J. R. astr. Soc.*, **29,** 289–318.

Solomon, S. & Sleep, N., 1974. Some simple physical models for absolute plate motions, *J. geophys. Res.*, **79,** 2557–2567.

Stauder, W., 1968a. Mechanism of the Rat island earthquake sequence of February 4, 1965, with relation to island arcs and sea-floor spreading, *J. geophys. Res.*, **73,** 3847–3858.

Stauder, W., 1968b. Tensional character of earthquake foci beneath the Aleutian trench and relation to sea-floor spreading, *J. geophys. Res.*, **73,** 7693–7702.

Stauder, W., 1972. Fault motion and spatially bounded character of earthquakes in Amchitka Pass and the Delarof Islands, *J. geophys. Res.*, **77,** 2072–2080.

Toksöz, M. & Kehrer, H., 1972. Tectonic strain-release characteristics of CANNIKIN, *Bull. seism. Soc. Am.*, **62,** 1425–1438.

Toksöz, M., Minear, J. & Julian, B., 1971. Temperature field and geophysical effects of a downgoing slab, *J. geophys. Res.*, **76,** 1113–1138.

Toksöz, M., Sleep, N. & Smith, A., 1973. Evolution of the downgoing lithosphere and the mechanisms of deep focus earthquakes, *Geophys. J. R. astr. Soc.*, **35,** 285–310.

Turcotte, D. & Schubert, G., 1973. Frictional Heating of the descending lithosphere, *J. geophys. Res.*, **78,** 5876–5886.
Turcotte, D. & Oxburgh, E., 1969. Convection in a mantle with variable physical properties, *J. geophys. Res.*, **74,** 1458–1474.
Walcott, R., 1970. Flexural rigidity, thickness, and viscosity of the lithosphere, *J. geophys. Res.*, **75,** 3941–3954.
Watts, A. & Talwani, M., 1974. Gravity anomalies seaward of deep-sea trenches and their tectonic implications, *Geophys. J. R. astr. Soc.*, **36,** 57–90.
Watts, A. & Talwani, M., 1975. Gravity effect of downgoing lithospheric slabs beneath island arcs, *Geol. Soc. Am. Bull.*, **86,** 1–4.
Wu, F. & Kanomori, A., 1973. Source mechanism of February 4, 1965, Rat island earthquake, *J. geophys. Res.*, **78,** 6082–6092.
Wyss, M. & Molnar, P., 1972. Source parameters of intermediate and deep focus earthquakes in the Tonga arc, *Phys. Earth Planet. Int.*, **6,** 279–292.

Appendix A

Numerical methods

The numerical methods used in this paper are based on Andrews (1972) with modifications necessary to handle non-linear rheology and for programming convenience. Because of the lengthy nature of the derivation, only those parts basic to the method or those modified are repeated.

For purposes of calculation the Boussinesq approximation and certain other assumptions normally made in mantle convection studies were adopted.

Assuming incompressible flow it is convenient to express the velocity of two-dimensional flow as the curl of a stream function, S.

$$u = \partial S/\partial y \tag{A1a}$$

$$v = -\partial S/\partial x \tag{A1b}$$

u horizontal velocity,

v vertical velocity,

x, y horizontal, vertical co-ordinates.

It is also convenient to remove the hydrostatic pressure due to overburden from the problem

$$p = P - \rho_0 g y \tag{A2}$$

ρ density,

ρ_0 density at ambient temperature in mantle $= 3{\cdot}3\ \mathrm{g\,cm^{-3}}$,

p excess pressure,

P total pressure,

g acceleration of gravity.

Since static support of the overburden produces no flow, the force on a surface can be represented by the excess pressure and stress deviators

$$f_{xx} = s_{xx} - p \tag{A3a}$$

$$f_y = s_{yy} - p \tag{A3b}$$

$$f_{xy} = f_{yx} = s_{xy} = s_{yx} \tag{A3c}$$

f_{xx}, f_{yy} force in x, y direction on surface normal to x, y.

s_{xx}, s_{yy}, s_{xy}, s_{yx} stress deviators

f_{xy}, f_{yx} shear stress in x, y direction on surface normal to y, x.

The stress deviators are

$$s_{xx} = -s_{yy} = 2\eta\,\partial u/\partial x = \frac{2\eta\,\partial^2 S}{\partial x \partial y} \tag{A4a}$$

$$s_{xy} = \eta\left(\frac{\partial u}{\partial y} + \frac{\partial v}{\partial x}\right) = \eta\left(\frac{\partial^2 S}{\partial y^2} - \frac{\partial^2 S}{\partial x^2}\right) \tag{A4b}$$

η viscosity.

Also it will be assumed that density varies linearly with temperature.

$$\rho = \rho_0(1-\alpha T) \tag{A5}$$

α coefficient of thermal expansion,

T temperature.

A more complex relationship between temperature and density could be easily included to represent phase changes.

The equations of equilibrium in terms of the stress deviators are

$$\frac{\partial s_{xx}}{\partial x} + \frac{\partial s_{xy}}{\partial y} - \frac{\partial p}{\partial x} = 0 \tag{A6}$$

$$\frac{\partial s_{xy}}{\partial x} + \frac{\partial s_{yy}}{\partial y} - \frac{\partial p}{\partial y} - \rho_0\, g\alpha T = 0. \tag{A7}$$

Eliminating pressure by taking the curl of these equations we obtain a single equation in terms of the stream function.

$$\frac{\partial^2}{\partial x \partial y}\left[4\eta\,\frac{\partial^2 S}{\partial x \partial y}\right] + \left(\frac{\partial^2}{\partial y^2} - \frac{\partial^2}{\partial x^2}\right)\left[\eta\left(\frac{\partial^2}{\partial x^2} - \frac{\partial^2}{\partial x^2}\right) S\right] - \frac{\partial}{\partial x}(\rho_0\, g\alpha T) = 0. \tag{A8}$$

The finite difference analog of (A8) used herein is self-adjoint and can be formulated from a variation principle (Andrews 1972):

$$\begin{aligned} S_0 = {} & [4(\eta_a+\eta_b+\eta_c+\eta_d)+\eta_E+\eta_N+\eta_W+\eta_S]^{-1} \\ & \times \{4[(\eta_d+\eta_a)S_E+(\eta_a+\eta_b)S_N+(\eta_b+\eta_c)S_W+(\eta_c+\eta_d)S_S] \\ & -(4\eta_a-\eta_E-\eta_N)S_{NE}-(4\eta_b-\eta_N-\eta_W)S_{NW} \\ & -(4\eta_c-\eta_W-\eta_S)S_{SW}-(4\eta_d-\eta_S-\eta_E)S_{SE} \\ & -(\eta_E\, S_{EE}+\eta_N\, S_{NN}+\eta_W\, S_{WW}+\eta_S\, S_{SS})-\rho_0\, g\alpha(T_e-T_w)/(\Delta x)^3\} \end{aligned} \tag{A9a}$$

where

$_0$ (subscript) point at which stream function is evaluated,

N, S (subscripts) points differing by ± 1 in y index

E, W (subscripts) points differing by ± 1 in x index

NE, SW, SE, NW points differing by ± 1 in both indexes

EE, NN, SS, WW points differing by ± 2 in one index

Δx grid spacing

e, w (subscripts) points $\pm\frac{1}{2}$ from 0 in x index

and

$$\eta_a \equiv (\eta_N + \eta_{NE} + \eta_0 + \eta_E), \tag{A9b}$$

$$\eta_b \equiv (\eta_{NW} + \eta_N + \eta_0 + \eta_W), \tag{A9c}$$

$$\eta_c \equiv (\eta_W + \eta_{SW} + \eta_0 + \eta_S), \tag{A9d}$$

$$\eta_d \equiv (\eta_E + \eta_{SE} + \eta_0 + S_S). \tag{A9e}$$

This equation was solved by pointwise relaxation. That is new values of the stream function at each point were obtained from the equation and the process repeated until a convergent solution was obtained. This slow process was improved by over-relaxation.

$$S_{NEW} = S_{OLD} + R(S'_{NEW} - S_{OLD}) \tag{A10}$$

where S'_{NEW} is the value obtained from equation (9) and R is a constant greater than 1. As an excessive value of R makes the process diverge at short wavelengths, there is a limit to the improvement which can be obtained.

Much more improvement was obtained extrapolating the progress of the solution over a large number of iterations. In this case S'_{NEW} is the value of the stream function after these iterations and S_{OLD} is the value before the iterations. A large value, enough to cut the convergence time to a fourth, of R then can be used. It is necessary to have a large number of iterations between intervals used for extrapolation since short wave errors must be removed so that the extrapolation samples the long wavelength error. This procedure gets around the problem of most relaxation methods in that the time to solve for the longest wavelength features is greatly reduced. Monitoring the progress of the iteration insures stability.

No work boundary

The 'no work' boundary condition can be obtained by noting that equation (A4) can be integrated to determine scalar pressure once stream function is known, as was done to obtain the hydrodynamic displacement of the free surface. If $\partial S/\partial y$, $\partial \eta/\partial y$ and $\partial^3 S/\partial y^3$ all vanish, $\partial p/\partial x$ in (A6) must be identically zero. Therefore, pressure is then constant along a boundary of constant h. As s_{xx} is also zero,

$$\begin{aligned} \text{Work} &= \int V \,.\, (p + s_{xx})\, dl \\ &= p \,.\, \int V\, dl = 0 \end{aligned} \tag{A11}$$

if all fluid enters and leaves by these boundaries.

Modelling showed that the boundary conditions for the asthenosphere could be changed to free slip on the bottom or no work on the landward side without significantly effecting the stress in the slab or the elevation.

Yield stress and viscosity

A non-linear visco-plastic rheology was assumed in several of the calculations in order to appraise the importance of non-linear effects. With this rheology a linear viscosity prevailed until a yield stress was exceeded by the total or invariant shear stress.

$$\tau = \mathrm{SQRT}(s_{xx}^2 + s_{xy}^2). \tag{A12}$$

This gives a simple non-linear rheology which is independent on co-ordinate system. The total shear stress was evaluated by using a nine-point finite different formula at each node

$$\tau = \eta_0\, \mathrm{SQRT}[\tfrac{1}{4}(S_{NE} + S_{SW} - S_{SE} - S_{NW})^2 + (S_N + S_S - S_E - S_W)^2]/\Delta x^2. \tag{A12b}$$

In the computer program, the yield stress was included by adjusting the viscosity at points where the stress was exceeded.

$$\eta_{NEW} = \tau_{YIELD}\, \eta_{OLD}/\tau_{OLD} \tag{A13}$$

and continuing the process with the solution of equation (A9) by relaxation until the solution converged. A solution thus found is indistinguishable from a solution which initially assumed as linear viscosities the apparent viscosities which were obtained. This procedure could be modified to include more complicated non-linear rheologies but was not so that rescaling could be possible.

Visco-elastic effects

Visco-elastic effects were not included as the primary interest was long term features such as elevation and gravity anomalies rather than individual deformations produced by earthquakes. The approach yields a time-averaged stress field rather than the stress field a number of years after the last major earthquake in a time-independent visco-elastic model (Smith & Toksöz 1972). In principle, time dependent visco-elastic models could be used to compute long term features, but the time increment is limited by the visco-elastic relaxation time of the least viscous material, about 10 years for the model assumed. This intractable procedure would add little insight, since individual elevation changes from earthquakes are small compared to the total topographic relief and individual apparent stress drop of earthquakes, 30 bars, are probably a small fraction of the total stress.

Convergence and accuracy

Convergence was evaluated by comparing the stream function and the surface elevation several thousand iterations apart. Certain runs which were relaxed significantly longer than others confirmed this procedure. After the calculation was initialised either from similar solution or by relaxation on a coarser grid, 20 000 to 100 000 iterations usually produced a stable answer if extrapolation was not used. Near the end of the iteration the solution was changing less than $10^{-6}\,\mathrm{cm^2\,s^{-1}}$ per iteration or about 1 part in 10^6. Because of the non-linear nature of several of the models, a method more sophisticated than relaxation, was not be used to solve the difference equation.

The effect of the error can be appraised by noting that the failure of the equation to exactly satisfy equation (A9) can be represented in terms of a spurious horizontal temperature gradient. From equation (A9) or from dimensional arguments, it can be derived that

$$\varepsilon = \rho_0\, g\alpha \Delta T_e\, \Delta x^3/20\eta \tag{A14}$$

ε failure of the stream function to fit difference equation, that is the change in the function in one iteration to the next by simple relaxation,

ΔT_e spurious horizontal temperature different across one zone.

For $\varepsilon = 10^{-6}\,\mathrm{cm^2\,s^{-1}}$, $\Delta x = 25\,\mathrm{km}$, $\alpha = 3\times10^{-5}\,^{\circ}\mathrm{C}^{-1}$, and $\eta = 10^{23}$ poise

$$\Delta T_e = 1{\cdot}3\times10^{6}\,^{\circ}\mathrm{C\,s^{-1}\,cm^{-2}}\,\varepsilon$$

As the change in stream function commonly was about or less than $10^{-6}\,\mathrm{cm^2\,s^{-1}}$ per iteration, an acceptable 1·3°C error results. Use of a larger viscosity for the lithosphere would have created problems in the non-linear models where the absolute values of the stream function were high. It can also be seen that a much more stringent convergence would be required if a finer grid had been used.

This need for a relatively coarse grid creates a problem of resolution, which is most serious for the crust of the island arc which is about 30 km. With a 25-km grid, the entire crust is included in one grid point. This results in approximating the 30-km crust with a thicker, less dense crust centred at 25 km. The tendency for the crust to spread is thereby increased (e.g. Artyushkov 1973, 1974). For preliminary calculations to define values of parameters this inaccuracy is not too severe. A finer grid must be used in models which seek to determine the details of processes in the crust of the island arc.

The numerical method used here was cross checked against a method modified after Burggraf (1966) in which a relaxation procedure where the stream function and the vorticity are simultaneously determined as two coupled harmonic equations.

Variable viscosity is included as a boundary condition between the upper and lower fluids. The expression for determining new values of the stream function on the boundary can be easily derived from the variational principle of minimum viscous dissipation analogous to that used by Andrews (1972). This derivation is lengthy and will not be given here.

Appendix B

Some seismic observations

Depth of the Aleutian earthquake of 1966 *June* 2

As noted in the text it is necessary to know the depth of earthquakes on the lip of the Aleutian trench to tell whether normal faulting is due to general tension in the plate or flexure. Body waves were used to determine depth because of a lack of suitable stations for surface wave measurements.

The earthquake of 1966 June 2 was selected for study because of the good quality of the short period records and because of the lack of interfering events. This and the earthquake of 1965 February 7 at 2.17 GMT differ from other normal faulting earthquakes in the Aleutians (see Stauder 1968b, 1972) by having clear impulsive short period *P*-waves. It is possible, therefore, that these events are not representative and perhaps occur at a much greater depth (Peter Molnar 1974, private communication).

Upon examination of WWSSN records revealed a clear depth phase of reversed polarity relative to *P*. The depth of the earthquake can be determined accurately for our purposes if this depth phase can be properly identified. For short period *P*-waves the strongest depth phases are *pP* (rock-water or sediment) and *pwP* (water-air) from oceanic events (Mendiguren 1971). If the event was shallow, *pP* would be lost in the coda and *pwP* would be the first obvious depth phase and be mistaken for *pP*.

To resolve this problem we note that the delays of possible phases *pP–P* and *pwP–P* vary distinctly with epicentral distance (Fig. 11). The delay *pP–P* is a much stronger function of distance and a better fit to the data. Given the scatter in the data this test is not by itself totally convincing. The residuals with respect to the *pP* curve are larger than the precision of the data and show some spatial coherence when plotted on a map of reflection points. We were not, however, able to more accurately locate the earthquake by comparing this result with observed topography.

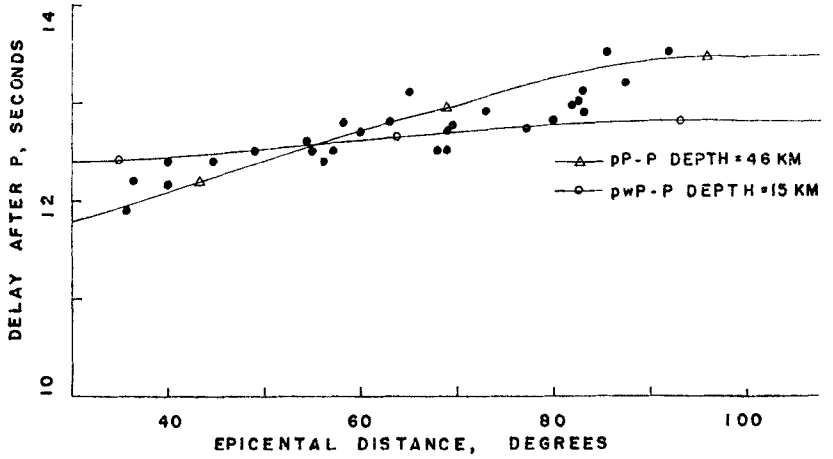

FIG. 11. Observed depth phase delays for the Aleutian earthquake of 1966 June 2 are plotted as a function of epicentral distance. The measurements are precise to about $\pm 0{\cdot}1$ s and data where confusion with *PcP* was likely to have been deleted. Theoretical delays for *pP* and *pwP* for 5·5 km water depth are shown (from Herrin 1968). Increasing the water depth would further flatten the *pwP* curve. The assumption that the depth phase is *pP* gives a better but not totally convincing fit to the data.

A second depth phase was observed about 8 s after the first at both long and short periods. The polarity and delay of this phase could not be determined to resolve *pwP* from *pwwP*. (These phases have opposite polarity. Late *pP* implies early *pwP*, while late *pwP* implies late *pwwP*.)

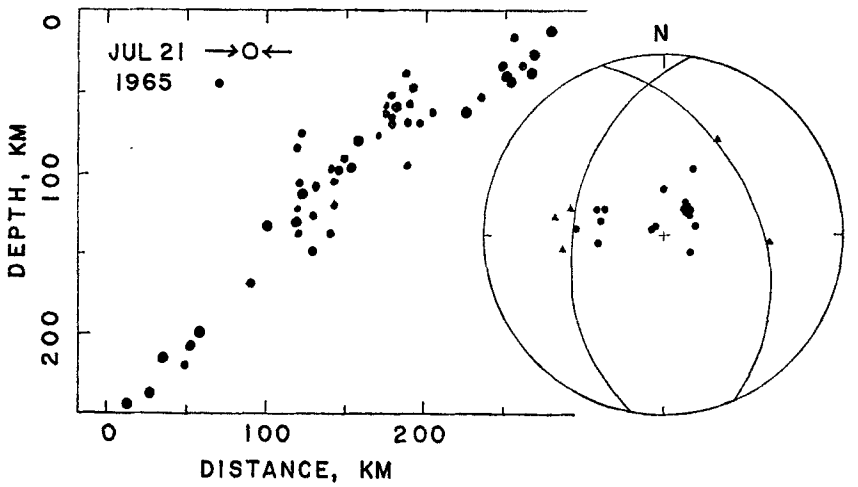

FIG. 12. Cross-section of the Tonga arc show the earthquake of 1965 July 21, in relation to other events (modified after Isacks *et al* 1969; Mitronavas *et al* 1969). Focal plane solution, lower hemisphere, was determined from WWSSN records and from ISC bulletin reports at local stations. A crustal velocity of 6·34 km s^{-1} was assumed at the source. Circles denote compressions and triangles dilatations.

S-wave data are also useful for determining depth, since sS–S is about 1·7 times pP–P. Marginal short-period *S* arrivals were noted at several stations at about 23 s after *S* and were compatible with the 46-km depth deduced from *P*-waves.

The weight of the evidence thus points to a location in the centre of the slab for this earthquake. Neither the *P*-wave or *S*-wave data by themselves are conclusive but combined they offer a reasonable solution. Short period records were valuable because precision was required. Long period records were useful in preliminary identification of the phases.

Mechanism of Tonga earthquake of 1965 *July* 21

Shallow events unrelated to the slab have been observed beneath the Aleutian arc. An event in an analogous position near Tonga (Fig. 12) was selected for study, as the small magnitude of the Aleutian events precludes teleseismic measurements. A first motion mechanism was constructed using long and short WWSSN records and bulletin arrivals at local stations. This event is clearly a thrust fault. The crustal velocity used to obtain orthogonal nodal planes and the planes themselves are constrained mainly by local unseen data and are thus somewhat suspect. The strike of the planes is parallel to the arc, however, as would be naively expected. This supports our inference that the shallow earthquakes beneath the arc are an extension of the thrust zone above the slab.